PAPER • OPEN ACCESS

Nonlinear distortion of intense THz beams

New Journal of Physics
The open access journal at the forefront of physics

Deutsche Physikalische Gesellschaft DPG
IOP Institute of Physics

Published in partnership with: Deutsche Physikalische Gesellschaft and the Institute of Physics

OPEN ACCESS

RECEIVED
7 April 2015

REVISED
1 July 2015

ACCEPTED FOR PUBLICATION
13 July 2015

PUBLISHED
19 August 2015

PAPER

Nonlinear distortion of intense THz beams

Cs Lombosi[1], **Gy Polónyi**[1], **M Mechler**[2], **Z Ollmann**[1], **J Hebling**[1,2] **and J A Fülöp**[1,2,3]

[1] Institute of Physics and Szentágothai Research Centre, University of Pécs, Ifjúság ú. 6 and 20, 7624 Pécs, Hungary
[2] MTA-PTE High-Field Terahertz Research Group, Ifjúság ú. 6, 7624 Pécs, Hungary
[3] ELI-ALPS, ELI-Hu Nkft., Dugonics tér 13, 6720 Szeged, Hungary

E-mail: fulop@fizika.ttk.pte.hu

Keywords: nonlinear optics, terahertz pulses, lithium niobate, optical rectification, tilted-pulse-front pumping

Abstract

Near- and far-field beam profiles were measured for THz pulses generated in $LiNbO_3$ by optical rectification of 200 fs pulses with a tilted pulse front. The variation of the THz beam size and a dramatically increasing divergence angle with increasing pump fluence were observed in the (horizontal) plane of the pulse front tilt. No significant variation was observed in the vertical direction. The reason for the observed nonlinear beam distortion is the shortening of the effective interaction length for THz generation caused by the combined effect of pump spectral broadening and angular dispersion in the tilted pulse front geometry. Our results indicate that nonlinear THz beam distortion effects have to be taken into account when designing intense THz sources and related experiments.

1. Introduction

The development of intense THz sources has gained breathtaking speed in the last few years. Primary attention was paid to the generation of ever higher THz pulse energies and field strengths. In the lower frequency part of the THz spectral range (0.1–2 THz), it was optical rectification pumped by femtosecond laser pulses with a tilted pulse front in $LiNbO_3$ (LN) [1] which had the leading role both in THz pulse energy and field strength. More than 0.4 mJ of energy [2] and 1.2 MV cm^{-1} peak electric field [3] have been reported. Efficiency as high as 3.8% has been reported from a cryogenically cooled LN source [4]. At higher (1–5 THz) frequencies, up to 0.9 mJ energy and 40 MV cm^{-1} have been reported from organic crystals [5].

As the energy of THz pulses increases, limitations of the efficiency inherent to the THz generation process become important [6, 7]. For example, the limiting effect of pump angular dispersion was investigated for THz sources using tilted pulse front pumping (TPFP) in LN [8, 9]. Saturation of the conversion efficiency was reported [10, 11] and pump self-phase modulation (SPM) was suggested as an explanation [11]. It was shown theoretically that the nonlinear interaction between the pump and THz fields can impose a strong limitation on the interaction length for THz generation [12], thereby quenching the efficiency.

While for many new applications it is important to increase the THz yield further [13–15], little attention has been paid so far to spatial characteristics of the generated THz beam, even though different methods are available for the measurement of beam properties [16–18]. The spatial emission characteristics of air plasma THz sources have recently been studied [18, 19], but less detailed experiments have been performed for TPFP in LN [20]. It was shown theoretically that distortions in the imaging system can lead to strongly distorted THz beam profiles [8], but possible nonlinear effects were not considered. As most applications of intense THz pulses involve focusing and beam transport optics, nonlinear THz spectroscopic and other high-field applications could highly benefit from careful consideration of possible THz beam distortions.

In this paper, we investigate the beam properties of the THz radiation emitted from an LN TPFP source with μJ-level energy. Strong variation of the THz beam divergence angle and the ellipticity of the beam cross section is observed with varying pump intensity. The observed nonlinear beam distortion effects are explained in terms of an intensity-dependent interaction length for THz generation. The results are important for the design of THz sources with μJ- and mJ-level energies, as well as for beam transport and focusing systems in related applications.

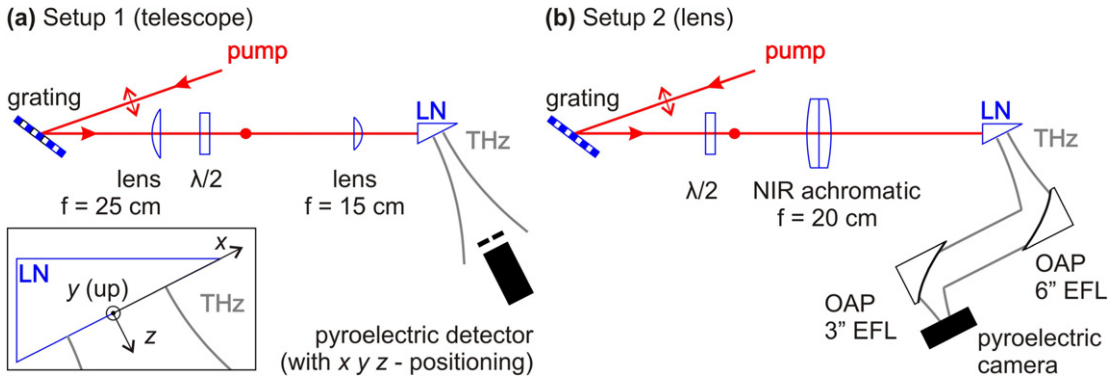

Figure 1. Experimental setup: (a) Setup 1 with the imaging telescope; (b) Setup 2 with the NIR achromatic lens. LN: $LiNbO_3$ prism, OAP: off-axis parabolic mirror, EFL: effective focal length. The inset in (a) shows the definition of the coordinate system.

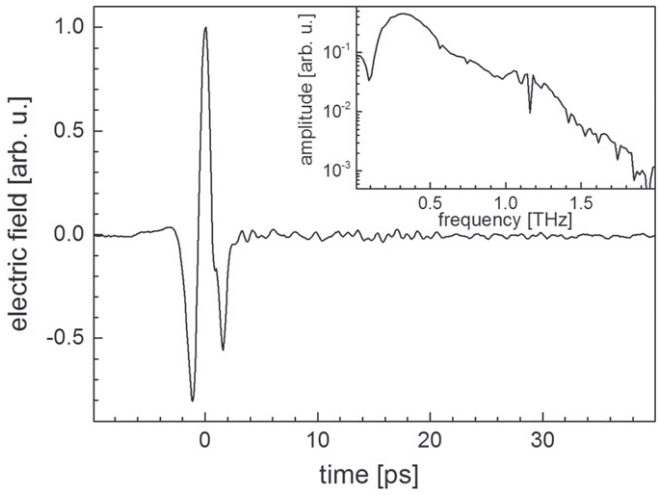

Figure 2. THz waveform measured by electro-optic sampling and the corresponding THz spectrum (inset).

2. Experimental setup

The pump laser, a diode-pumped Yb:CaF_2 regenerative amplifier (Amplight) with a repetition rate of 1 kHz, delivered 200 fs pulses at a central wavelength of 1030 nm. THz pulses were generated in a 0.6% MgO-doped stoichiometric LN prism at room temperature using TPFP. Two different pulse front tilting systems were used. In Setup 1 (figure 1(a)) a 1400 lines mm^{-1} grating was used to tilt the pump pulse front. The polarization direction of the diffracted pump beam was rotated from horizontal to vertical (parallel to the optical axis of the LN crystal) by a $\lambda/2$ retardation plate. Optimal imaging conditions [2, 8] were provided by a telescope consisting of a 25 cm and a 15 cm focal length lens in a confocal arrangement. The maximum pump energy at the LN crystal was 5.8 mJ, and the $1/e^2$ pump spot diameter was 3.8 mm × 5.6 mm (horizontal × vertical). The maximum pump fluence was about 35 mJ cm^{-2}, the corresponding intensity was 177 GW cm^{-2}. In Setup 2 (figure 1(b)), the imaging telescope was replaced by a 20 cm focal length near-infrared (NIR) achromatic lens. The maximum pump energy at the LN crystal was 6.3 mJ, and the pump spot diameter was 4.0 mm × 4.9 mm, giving a maximum pump fluence of 41 mJ cm^{-2} and a 205 GW cm^{-2} intensity.

THz pulses of up to 9 μJ energy were generated with a maximum efficiency of 0.15%, measured by a calibrated pyroelectric detector (Microtech Instruments). The temporal waveform of the THz pulses (figure 2) was measured by electro-optic sampling using a 0.1 mm thick, (110)-oriented ZnTe crystal on a 2 mm thick inactive ZnTe substrate. The spectral peak was at 0.33 THz (figure 2, inset).

Horizontal (x-axis) and vertical (y-axis) cross sections of the THz beam profile were measured both in Setup 1 and 2 by using a sensitive, large-area pyroelectric detector (Gentec QS9-THz-BL, figure 1(a)) with xyz-positioning capability. A variable-aperture iris diaphragm was placed in front of the detector. In order to restrict

spatial averaging effects, at each z-position an aperture size between 5% and 20% of the $1/e^2$ THz beam diameter was chosen, depending on the signal level. High detector sensitivity was essential to enable measurements with small aperture openings and at large distances from the source. Black cardboard sheets and a 0.5 mm thick silicon wafer were used to block the pump radiation and its second harmonic from entering the detector. Two-dimensional near-field THz beam profiles in Setup 2 were measured using a pyroelectric camera (Ophir Pyrocam III), where the output surface of the LN crystal was imaged with 2:1 demagnification on the camera by two off-axis parabolic mirrors (figure 1(b)). The effective focal lengths of the 2″-diameter parabolas were 6″ and 3″, respectively.

3. Results

3.1. THz beam divergence

In the first measurement series, we investigated the horizontal (x) and vertical (y) cross sections of the THz beam profile at various distances up to $z = 430$ mm from the output surface of the LN crystal ($z = 0$, see inset in figure 1). All profile measurements were carried out at a few different pump intensity levels, both for Setup 1 and Setup 2. The experimental findings are summarized in figure 3. Examples of the measured horizontal far-field beam profiles are shown in figures 3(a) and (b) for $z = 310$ mm. For both setups, the THz beam width increases dramatically with increasing pump fluence. This increase is stronger for Setup 1 (telescope).

The beam profile measurements enabled the determination of the THz beam divergence in the horizontal and vertical directions. For simplicity, we assumed Gaussian beam propagation to fit the measured beam profiles for the determination of the horizontal and vertical beam radii $W_H(z)$ and $W_V(z)$, respectively, as well as the divergence angles $\theta_{0,H}$ and $\theta_{0,V}$ defined as asymptotic half opening angles of the beam [21]. A frequency of 0.33 THz was used in beam propagation fitting, corresponding to the measured THz spectral peak (figure 2, inset). The position and size of the beam waist were the optimization parameters. The horizontal and vertical beam radii obtained from fitting at different propagation distances can be seen in figures 3(c) and (e) for Setup 1 (telescope), and in figures 3(d) and (f) for Setup 2 (lens), respectively, together with the fitted $W_H(z)$ and $W_V(z)$ curves.

The THz beam divergence in the horizontal plane increased dramatically with increasing pump fluence (figures 3(c) and (d)), while it remained essentially unchanged in the vertical plane (figures 3(e) and (f)). For example, in the case of Setup 1 (telescope) at the lowest pump fluence (5.4 mJ cm^{-2}) a horizontal divergence angle of 5.1° was obtained, which increased to 12.9° at the highest fluence (35.4 mJ cm^{-2}) (figure 3(c)). In contrast, the vertical divergence angle remained in the range of 4°–6° for all pump fluence levels (figure 3(e)). Similar behavior was observed with Setup 2 (lens). In this case, the variation of the horizontal divergence angle was slightly smaller, starting from 5.9° at 6.6 mJ cm^{-2} and increasing to 10.4° at 41 mJ cm^{-2} (figure 3(d)). One possible reason for this could be the difference in imaging distortions of the two setups, which can lead to different pump pulse fronts, and consequently THz phase front curvatures [8].

3.2. Near-field THz beam profiles

In another measurement series, we investigated the two-dimensional near-field THz intensity beam profile at various pump fluence levels by imaging the output surface of the LN crystal using a pyroelectric camera in Setup 2 (lens, figure 1(b)). The demagnification of the off-axis parabolic mirror pair was 2:1. Examples of the measured THz beam profiles are shown in figure 4, rescaled to compensate for demagnification. At low pump fluence (8.6 mJ cm^{-2}) the THz spot is elliptical with $1/e^2$ half-widths of $W_H = 2.5$ mm and $W_V = 1.8$ mm in the horizontal and vertical directions, respectively (figure 4(a)). This corresponds to an axis ratio of $W_H/W_V = 1.38$. At the highest pump fluence (31.8 mJ cm^{-2}), the THz spot has a reduced horizontal half-width of $W_H = 2.1$ mm, while in the vertical direction the spot half-width remained essentially the same $W_V = 1.8$ mm (figure 4(b)). This corresponds to a reduced axis ratio of $W_H/W_V = 1.19$. In addition, a horizontal shift of the THz beam center by about 1 mm can be observed in the $-x$ direction (figure 1, inset), while the center position did not change in the vertical (y) direction.

Figure 5(a) shows the measured THz spot size as a function of the pump fluence. A monotonic decrease in the horizontal spot size was observed, changing from about 2.5 mm at 5.3 mJ cm^{-2} to about 2.1 mm at 31.8 mJ cm^{-2}, as mentioned above. The vertical size remained essentially unchanged. We note that such an intensity-dependent variation of the near-field THz beam profile is in accordance with the observed variation of the beam divergence. Figure 5(b) shows the horizontal and vertical beam center positions as a function of the pump fluence. The center positions were determined as center-of-mass (centroid) positions. In the horizontal direction, a monotonic shift can be seen towards the crystal apex, corresponding to the $-x$ direction (figure 1, inset). The maximum shift is about −1 mm with respect to the position at the lowest pump fluence. The vertical position remained essentially unchanged.

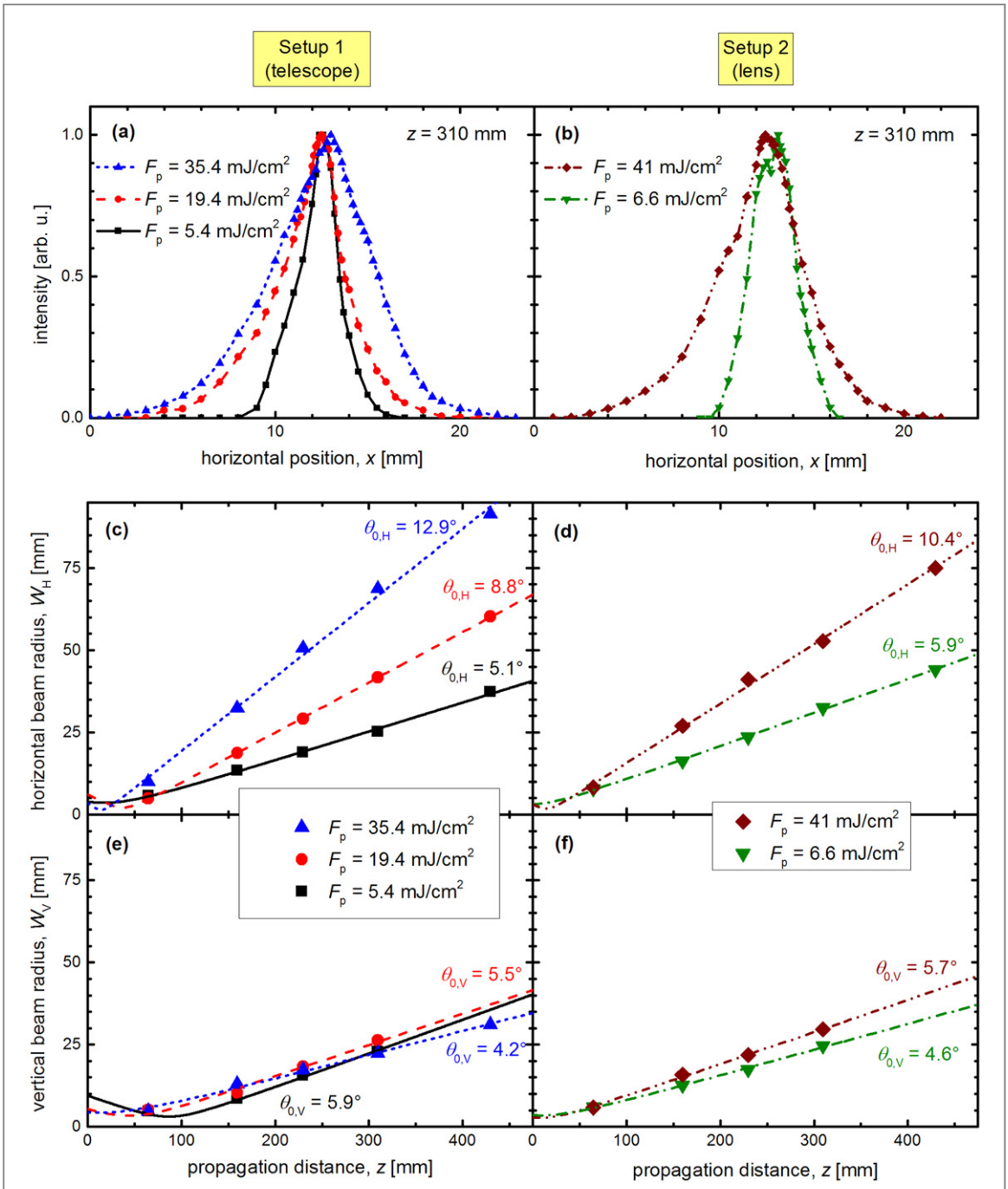

Figure 3. Examples of measured THz beam profiles for different pump intensities at $z = 310$ mm for Setup 1 (a) and Setup 2 (b). Observed variation of horizontal (c) and vertical (e) THz beam radii as a function of the propagation distance z for Setup 1 (telescope). (d), (f) show the corresponding radii for Setup 2 (lens).

4. Discussion

Both the THz divergence and the near-field THz beam profile measurements presented above show the variation of the THz beam in the horizontal direction with varying pump fluence, while the beam properties in the vertical direction remained essentially unchanged. The observed behavior can be explained in terms of an effective interaction length for THz generation, which is dependent on the pump fluence.

The effective interaction length for THz generation L_{eff}, introduced in [8], can be defined as the distance measured in the THz propagation direction over which the THz intensity grows from 5% to its peak value. For large diameter pump beams and small pump intensities this is determined by the variation of the pump pulse duration (and therefore of the pump intensity) with the propagation distance due to material and angular dispersions, and by the absorption at THz frequencies [8, 9]. Therefore, in this case, there is a close relation between L_{eff} and the double dispersion length $2L_{\text{d}}$. The double dispersion length gives the propagation distance,

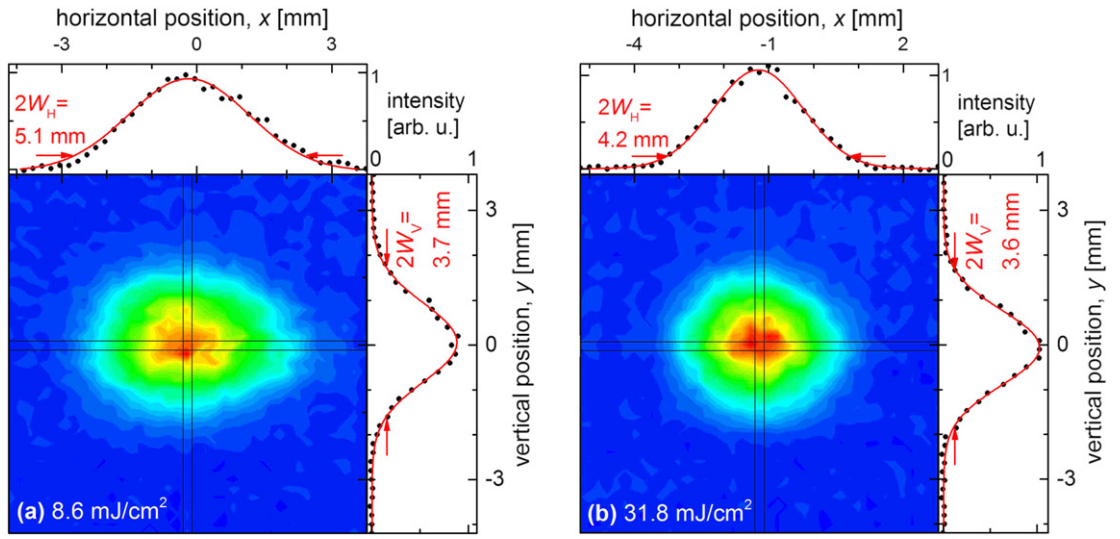

Figure 4. Measured two-dimensional near-field THz intensity beam profiles at (a) 8.6 mJ cm^{-2} and (b) 31.8 mJ cm^{-2} pump fluence. The insets show the respective central one-dimensional profiles.

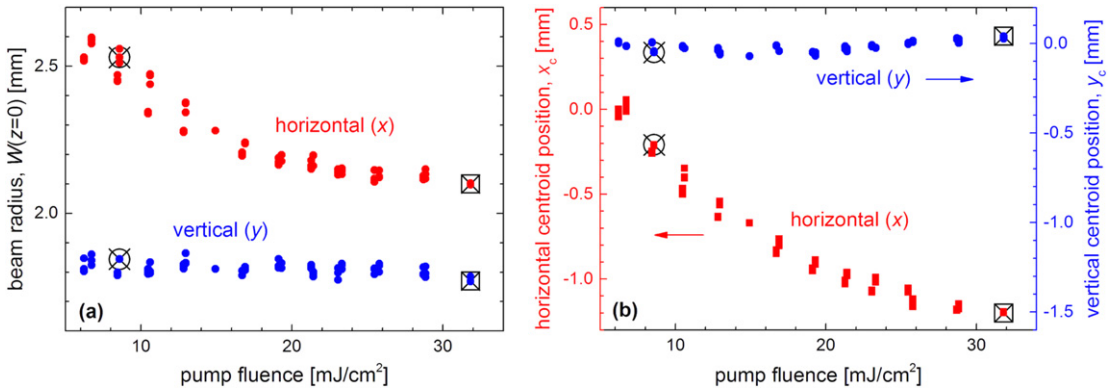

Figure 5. Measured horizontal and vertical near-field THz beam radii (a) and positions of near-field THz beam centroid (b) as a function of the pump fluence. The data points with the crossed circle and square symbols correspond to the beam profiles in figures 4(a), (b), respectively.

where the pump pulse duration does not exceed $\sqrt{2}\,\tau_0$ with τ_0 being the Fourier-limited pulse duration (see also figure 2 of [8]).

At larger pump intensities, the generated THz field can be strong enough to significantly modify the pump spectrum [12, 22, 23]. In addition, the pump pulse can also be influenced by SPM [11]. In order to assess the influence of such effects on the dispersion and interaction lengths, we carried out numerical simulations by solving the one-dimensional coupled wave equations for the pump and the THz fields. The model, similar to that described in [12], takes into account (i) the variation of the pump pulse duration (and therefore of the pump intensity) with the propagation distance due to material dispersion and angular dispersion, (ii) the non-collinear propagation direction of the pump and THz beams, (iii) the absorption at THz frequencies due to the complex dielectric function (determined by phonon resonances), (iv) the effect of the generated THz field on the pump field (i.e. sum- and difference-frequency generation between the optical and the THz fields), and (v) pump SPM. In the simulations, pump pulses with Fourier-limited pulse duration of 200 fs were assumed. The initial chirp was set to shift the position of the Fourier-limited pulse duration to the middle of the LN crystal. The maximum THz propagation distance inside the LN crystal was set to about 2.3 mm in the z-direction, approximately corresponding to the experimental situation for the beam center.

Figure 6(a) shows the variation of the pump pulse duration inside the LN crystal as a function of the THz propagation coordinate z for various pump fluence levels. At the lowest (0.037 mJ cm^{-2}) pump fluence, it is dominated by the effect of angular dispersion (black solid curve in figure 6(a)). As the fluence is increased, the nonlinear coupling between THz and optical fields (and to a smaller extent SPM) leads to increasing broadening

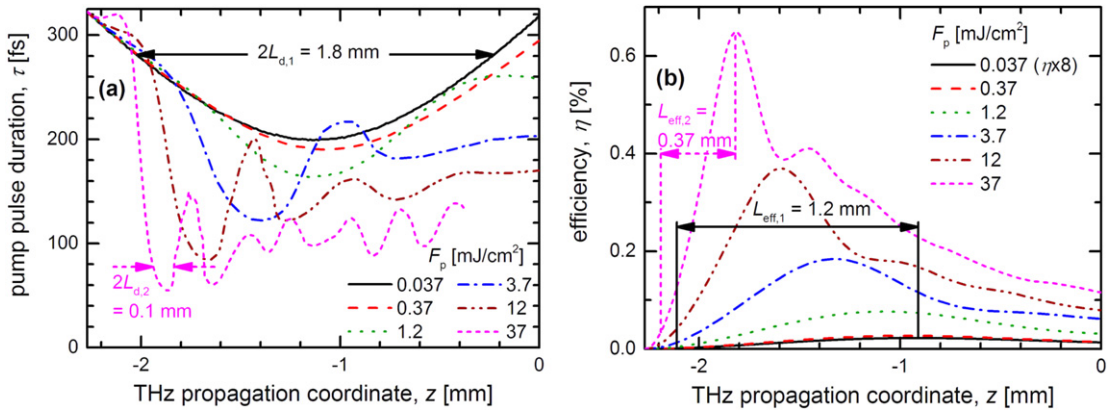

Figure 6. Pump pulse duration (a) and pump-to-THz energy conversion efficiency (b) versus THz propagation length for various pump fluence levels.

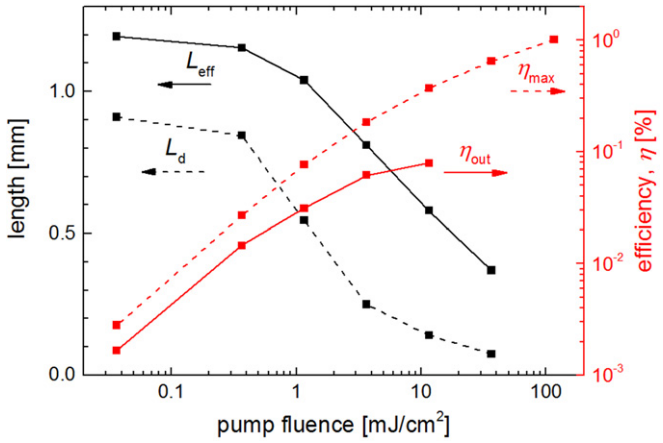

Figure 7. The dispersion length L_d, the interaction length L_{eff}, the maximum efficiency η_{max}, and the output efficiency η_{out} as a function of the pump fluence.

of the pump spectra (not shown). The combined effect of spectral broadening and angular dispersion leads to a rapidly decreasing pulse duration well below the original Fourier limit. This is shown by the curves in figure 6(a) corresponding to higher pump fluence values. After reaching its minimum, an oscillatory variation of the pulse duration can be seen. The minimum pulse duration decreases from the original 200 fs Fourier limit at the lowest fluence to as short as 55 fs at the highest (37 mJ cm^{-2}) fluence. The corresponding double dispersion length $2L_d$ decreases from 1.8 mm to as little as 0.1 mm, the interaction length L_{eff} decreases from 1.2 mm to 0.37 mm (figure 6; see also figure 7).

Figure 6(b) shows the corresponding variation of the pump-to-THz conversion efficiency η along the THz propagation coordinate z. While the peak efficiency η_{max} increases with increasing pump fluence, the effective interaction length L_{eff} decreases (figure 6(b); see also figure 7), in close correspondence with the dispersion length L_d (figure 6(a); see also figure 7). The variation of the dispersion and the interaction lengths, and that of the peak and output efficiencies as a function of the pump fluence is plotted in figure 7.

Based on the simulation results, a qualitative explanation for the observed behavior of the THz beam profile can be given as follows. (Two-dimensional simulations are required for more accurate, quantitative modeling of the experimental findings.) With increasing intensity, the dispersion length, and correspondingly, the effective length for THz generation decrease (figure 7). This results in reduction of the thickness of the THz-generating active region, with its center shifting away from the output surface of the LN prism (figure 8). As indicated in the figure, the consequence is the reduction of the THz beam size in the horizontal (x) direction, accompanied by a shift in the THz beam center. No change in the beam profile is expected in the direction vertical to the plane of the non-collinear phase matching (y-direction). The reduced near-field horizontal THz beam size leads to an increased THz beam divergence at higher pump fluences, in accordance with the measurements.

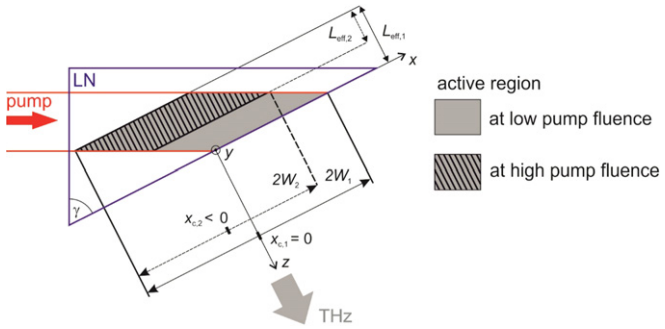

Figure 8. Horizontal beam size variation and beam center shift originating from the combined effect of intensity-dependent interaction length and the non-collinear phase-matching geometry.

5. Conclusion

Near-field and far-field THz beam profiles and THz divergence angles were measured for a TPFP LN source pumped by 200 fs laser pulses. The horizontal near-field beam diameter was observed to be decreasing and the corresponding divergence angle increased with increasing pump fluence. No significant change was found in the vertical direction. One-dimensional model calculations revealed the strong decrease of the pump dispersion length and the interaction length for THz generation with increasing pump fluence. The observed nonlinear behavior of the THz beam properties was qualitatively explained by the interplay between the intensity-dependent interaction length and the non-collinear phase-matching geometry of the TPFP scheme.

Our results clearly show that besides optimizing the efficiency of intense THz sources, special care has to be taken in relation to the THz beam properties. The observed dependence of the THz beam properties on the pump fluence is highly relevant for designing THz sources and application setups, which include focusing or beam transport lines, and measurement setups with variable pump intensity. The large nonlinear variation of the beam divergence can also seriously affect the spectral transmission of optical systems with limited aperture. Our results are important for the rapidly developing research fields of THz nonlinear spectroscopy and high-field THz science.

Acknowledgments

Financial support from the Hungarian Scientific Research Fund (OTKA) grant numbers 101846 and 113083 is acknowledged. JAF acknowledges support from a János Bolyai Research Scholarship (Hungarian Academy of Sciences). The present scientific contribution is dedicated to the 650th anniversary of the foundation of the University of Pécs, Hungary.

References

[1] Hebling J, Almasi G, Kozma I Z and Kuhl J 2002 Velocity matching by pulse front tilting for large area THz-pulse generation *Opt. Express* **10** 1161–6
[2] Fülöp J A, Ollmann Z, Lombosi C S, Skrobol C, Klingebiel S, Pálfalvi L, Krausz F, Karsch S and Hebling J 2014 Efficient generation of THz pulses with 0.4 mJ energy *Opt. Express* **22** 20155–63
[3] Hirori H, Doi A, Blanchard F and Tanaka K 2011 Single-cycle terahertz pulses with amplitudes exceeding 1 MV cm^{-1} generated by optical rectification in $LiNbO_3$ *Appl. Phys. Lett.* **98** 091106
[4] Huang S-W, Granados E, Ronny Huang W, Hong K-H, Zapata L E and Kärtner F X 2013 High conversion efficiency, high energy terahertz pulses by optical rectification in cryogenically cooled lithium niobate *Opt. Lett.* **38** 796–8
[5] Vicario C, Ovchinnikov A V, Ashitkov S I, Agranat M B, Fortov V E and Hauri C P 2014 Generation of 0.9 mJ THz pulses in DSTMS pumped by a Cr:Mg_2SiO_4 laser *Opt. Lett.* **39** 6632–5
[6] Wu X, Carbajo S, Ravi K, Ahr F, Cirmi G, Zhou Y, Mücke O D and Kärtner F X 2014 Terahertz generation in lithium niobate driven by Ti:sapphire laser pulses and its limitations *Opt. Lett.* **39** 5403–6
[7] Blanchard F, Ropagnol X, Hafez H, Razavipour H, Bolduc M, Morandotti R, Ozaki T and Cooke D G 2014 Effect of extreme pump pulse reshaping on intense terahertz emission in lithium niobate at multimilliJoule pump energies *Opt. Lett.* **39** 4333–6
[8] Fülöp J A, Pálfalvi L, Almási G and Hebling J 2010 Design of high-energy terahertz sources based on optical rectification *Opt. Express* **18** 12311–27
[9] Fülöp J A, Pálfalvi L, Hoffmann M C and Hebling J 2011 Towards generation of mJ-level ultrashort THz pulses by optical rectification *Opt. Express* **19** 15090–7
[10] Fülöp J A, Pálfalvi L, Klingebiel S, Almási G, Krausz F, Karsch S and Hebling J 2012 Generation of sub-mJ terahertz pulses by optical rectification *Opt. Lett.* **37** 557–9

[11] Bodrov S B, Murzanev A A, Sergeev Y A, Malkov Y A and Stepanov A N 2013 Terahertz generation by tilted-front laser pulses in weakly and strongly nonlinear regimes *Appl. Phys. Lett.* **103** 251103
[12] Ravi K, Huang W R, Carbajo S, Wu X and Kärtner F 2014 Limitations to THz generation by optical rectification using tilted pulse fronts *Opt. Express* **22** 20239–51
[13] Hebling J, Fülöp J A, Mechler M I, Pálfalvi L, Tőke C and Almási G 2011 Optical manipulation of relativistic electron beams using THz pulses arXiv: 1109.6852
[14] Wong L J, Fallahi A and Kärtner F X 2013 Compact electron acceleration and bunch compression in THz waveguides *Opt. Express* **21** 9792–806
[15] Pálfalvi L, Fülöp J A, Gy T and Hebling J 2014 Evanescent-wave proton postaccelerator driven by intense THz pulse *Phys. Rev. ST Accel. Beams* **17** 031301
[16] Reiten M T, Harmon S A and Alan Cheville R 2003 Terahertz beam propagation measured through three-dimensional amplitude profile determination *J. Opt. Soc. Am.* B **20** 2215–25
[17] Molloy J F, Naftaly M and Dudley R A 2013 Characterization of terahertz beam profile and propagation *IEEE J. Sel. Top. Quantum Electron.* **19** 8401508
[18] Oh T I, Yoo Y J, You Y S and Kim K Y 2014 Generation of strong terahertz fields exceeding 8 MV/cm at 1 kHz and real-time beam profiling *Appl. Phys. Lett.* **105** 041103
[19] Klarskov P, Strikwerda A C, Iwaszczuk K and Jepsen PU 2013 Experimental three-dimensional beam profiling and modeling of a terahertz beam generated from a two-color air plasma *New J. Phys.* **15** 075012
[20] Klarskov P, Strikwerda A C, Wang T, Zalkovskij M and Jepsen P U 2013 3D terahertz beam profiling *Proc. SPIE* **8624** 86240D
[21] Saleh B E A and Teich M C 1991 *Fundamentals of Photonics* (New York: Wiley) ch 3
[22] Hattori T and Takeuchi K 2007 Simulation study on cascaded terahertz pulse generation in electro-optic crystals *Opt. Express* **15** 8076–93
[23] Jewariya M, Nagai M and Tanaka K 2009 Enhancement of terahertz wave generation by cascaded $\chi^{(2)}$ processes in $LiNbO_3$ *J. Opt. Soc. Am.* B **26** A101–06